Altered Huntingtin-Chromatin Interactions Predict Transcriptional and Epigenetic Changes in Huntington's Disease Mouse Models

Jocelynn R Pearl * (1,2), Amol C Shetty * (3), Jeffrey P Cantle * (4,5), Dani E Bergey (1), Robert M. Bragg (4,5), Sydney R. Coffey (4), Holly B. Kordasiewicz (6), Leroy E Hood (1,7,8), Nathan D Price (1,7,9), Seth A Ament (3,10) **, Jeffrey B Carroll (4,5) **

1. Institute for Systems Biology, Seattle, Washington
2. Molecular & Cellular Biology Graduate Program, University of Washington, Seattle, Washington
3. Institute for Genome Sciences, University of Maryland School of Medicine, Baltimore, MD
4. Behavioral Neuroscience Program, Department of Psychology, Western Washington University, Bellingham, Washington
5. Department of Neurology, University of Washington, Seattle, WA, USA
6. Ionis Pharmaceuticals, Carlsbad, CA
7. Buck Institute for Research on Aging, Novato, CA
8. Phenome Health, Seattle, WA
9. Thorne HealthTech, New York, NY
10. Maryland Psychiatric Research Center, Department of Psychiatry, University of Maryland School of Medicine, Baltimore, MD

* Co-First

**co-corresponding authors: jeffcarr@uw.edu / SAment@som.umaryland.edu

Abstract

Progressive striatal gene expression changes and epigenetic alterations are a prominent feature of Huntington's disease (HD), but the mechanistic basis remains poorly understood. Using chromatin immunoprecipitation and sequencing (ChIP-seq), we show that the huntingtin protein (HTT) reproducibly occupies specific locations in the mouse genome. Moreover, many genomic loci were differentially occupied by HTT in striatal tissue from a homozygous knock-in mouse model of HD (B6.*Htt*$^{Q111/Q111}$) when compared to wildtype controls. Huntingtin ChIP-seq peaks were enriched in the coding regions of cell identity genes important for striatal function, with many of these genes found to have reduced expression in the striata of HD patients and mouse models, as well as reduced HTT occupancy in *Htt*$^{Q111/Q111}$ mice compared to controls. Conversely, HTT ChIP-seq peaks were depleted near genes that are up-regulated in HD. ChIP-seq of bulk striatal histone modifications, generated in parallel, revealed genotype-specific colocalization of HTT with active chromatin marks (H3K4me3 and H3K27ac), and with enhancer of zeste homolog 2 (EZH2), a key enzymatic component of the PRC2 complex. Near genes that are differentially regulated in HD, greater HTT occupancy in *Htt*$^{Q111/Q111}$ vs. wildtype mice was associated with increased EZH2 binding, increased histone H3 lysine 4 (H3K4me3), and decreased histone H3 lysine 27 (H3K27me3). Our study suggests that huntingtin-chromatin interactions may play a direct role in organizing chromatin and promoting cell type-specific gene expression, with loss of HTT occupancy predicting decreased gene expression in HD.

Keywords

huntington's disease, huntingtin, chromatin, epigenetics

Introduction

Huntington's disease (HD) is a fatal dominant neurodegenerative disease caused by expansion of a glutamine-coding (polyQ) CAG tract near the 5' end of the *Huntingtin* (*HTT*) gene[1]. Clinical symptoms include

50 deficits in motor control and cognition, as well as psychiatric symptoms. HD progression is linked to the
51 selective death of spiny projection neurons (SPNs) in the striatum[2]. Transcriptional[3] and epigenomic[4–7]
52 dysregulation are among the earliest phenotypes in cells and tissues expressing mutant HTT protein (mHTT)
53 and are highly reproducible in brain tissue from humans with HD[8–10]. However, the molecular mechanisms
54 by which mHTT mediates these transcriptional changes are poorly understood.

55 A straightforward hypothesis is that HTT directly contributes to transcriptional dysregulation in HD
56 through interactions with chromatin-bound DNA. In the cell, HTT protein dynamically shuttles between the
57 cytoplasm and nucleus[11]. Mis-localization of mHTT to the nucleus is an early phenotype in HD animal
58 models, roughly coincident with the onset of transcriptional changes, and is a critical driver of mHTT-mediated
59 neuronal death, both *in vitro* and in mouse models[11–13]. To date, specific interactions of HTT with chromatin
60 remain obscure, but they are supported by several lines of indirect evidence: (i) chromatin immunoprecipitation
61 indicates that HTT affiliates with chromatin DNA[14]; (ii) the HTT protein contains a series of HEAT domains,
62 which are capable of serving as DNA binding domains[15]; and (iii) HTT forms direct protein-protein
63 interactions with a variety of transcriptional regulatory proteins in the nucleus, including transcription factors
64 (TFs) and chromatin remodeling factors[16]. Perhaps the best understood of such interactions involve
65 chromatin remodeling complexes that mediate gene repression and heterochromatin formation. HTT binds in a
66 polyQ-length sensitive manner to polycomb repressive complex 2 (PRC2), the chromatin remodeling complex
67 responsible for trimethylation of lysine 27 on the histone 3 tail (H3K27me3), a repressive mark associated with
68 bi-valent, or poised chromatin regions that are critical to developmental fate commitment[17]. Ablation of PRC2
69 in SPNs reproduces several of the cellular phenotypes in HD, including aberrant de-repression of transcripts
70 that code for developmentally regulated transcription factors, loss of SPN identity gene expression, and
71 prolonged cell death[18]. We[19] and others[4,10] have observed that a common transcriptional feature of HD
72 is a reduction of cell-type appropriate gene expression, providing additional impetus to understand changes in
73 PRC2 function in HD, given its key role in the regulation of cell fate[20].

74 To investigate the hypothesis that HTT occupies specific locations on chromatin DNA, we performed
75 chromatin immunoprecipitation and deep sequencing (ChIP-seq) to map HTT genomic occupancy in striatal
76 tissue from the $Htt^{Q111/Q111}$ knock-in mouse model of the HD mutation and in wildtype $Htt^{+/+}$ controls. We
77 analyzed these data together with publicly available RNA-seq and with newly generated ChIP-seq of the

78 histone modifications H3K27me3, H3K9me3 and H3K4me3, and the PRC2 histone methyltransferase effector
79 subunit EZH2, generated in parallel from the striatum of age-matched of *Htt*$^{Q111/+}$ mice. We describe thousands
80 of reproducible HTT ChIP-seq peaks, both in *Htt*$^{+/+}$ and *Htt*$^{Q111/Q111}$ mice, and observe robust genotype-specific
81 patterns of occupancy, which are correlated with epigenetic and transcriptional changes seen in HD. These
82 results provide, for the first time, a genome-wide map of HTT genomic occupancy and suggest that altered
83 transcription in HD arises, in part, via alterations in direct HTT-chromatin interactions.
84

85 Results

86 HTT Reproducibly Occupies Thousands of Locations in the Mouse Genome

87 We set out to map the genomic occupancy of HTT and assess its relationship to HD mutations in the
88 striatum of *Htt*$^{Q111/Q111}$ and wildtype mice. *Htt*^{Q111} is a well-characterized, genetically precise knock-in mouse
89 model of a mutation associated with juvenile-onset HD, in which a human allele of *HTT* exon 1 with
90 approximately 111 glutamine-encoding CAG repeats has been inserted into the endogenous mouse *Htt* locus.
91 For maximal fidelity to genetics of human HD patients, most studies utilize heterozygous *Htt*$^{Q111/+}$ mice.
92 However, for HTT ChIP-seq experiments homozygous *Htt*$^{Q111/Q111}$ mice are preferred to avoid the confound of
93 two isoforms of HTT being present in each sample. HD is inherited in a fully dominant fashion, and HD patients
94 with compound heterozygous HD mutations generally experience symptoms equivalent to heterozygous
95 patients with a single mutant allele. Likewise, the progression of disease-related phenotypes is comparable in
96 heterozygous *Htt*$^{Q111/+}$ mice and *Htt*$^{Q111/Q111}$ homozygotes, with four months of age representing an early time
97 point. At this age, we[8,21] and others[10] have detected hundreds of differentially expressed genes in striatal
98 tissue and misfolded HTT isoforms in the nuclei of many striatal SPNs from *Htt*$^{Q111/+}$ mice, but there is not yet
99 any discernible striatal cell death or glial proliferation[21]. Chromatin immunoprecipitation and deep sequencing
100 (ChIP-seq) was performed using striatal tissue from four-month-old *Htt*$^{Q111/Q111}$ and wildtype mice, using a well-
101 validated antibody, EPR5526[22], which recognizes an N-terminal epitope of the HTT protein with no known
102 differences in affinity for wildtype vs. mutant HTT isoforms. We sequenced three biological replicates from

103 *Htt*$^{Q111/Q111}$ mice and three from *Htt*$^{+/+}$ mice, with each biological replicate consisting of pooled striata from three
104 mice (Fig. 1A).

105 Initial inspection suggested that HTT occupies broad domains along chromatin DNA (e.g. Fig. 1C-D).
106 We conducted peak-calling using `MACS`[23] in broad peak mode, which revealed 9,656 reproducible peaks, of
107 which 9,624 peaks were not overlapping blacklisted regions and 4,900 peaks were conditionally reproducible,
108 i.e. identified independently in at least two biological replicates from each genotype (Fig. 1B; Tables S1 and
109 S2). Reproducible HTT peaks (HTT, mHTT, and shared) were found in both genic and intergenic regions: 0.1%
110 in the 5' UTR, 31% within 3kb upstream of TSS, 1.1% in the first exon, 3.6% in other exons, 10.7% in the first
111 intron, 28.1% in other introns, 4.4% in the 3' UTR, with 20.8% ≤ 300kb downstream or in distal intergenic
112 regions (Fig. 4A). A HTT-sequence-specific control experiment supports the hypothesis that these regions
113 accurately reflect HTT occupancy rather than non-specific signals. Namely, we observe fewer HTT ChIP-seq
114 peaks in brain tissue from mice treated with an antisense oligonucleotide (ASO) to reduce HTT levels in the
115 brain (Fig. S1).

116 Robust HTT peaks were found within 1 Mb of 2,628 protein-coding genes. Importantly, most genes do
117 not contain HTT binding sites, suggesting that HTT occupancy in the vicinity of a given gene may reflect a
118 specific regulatory role limited to this subset of genes, rather than promiscuous binding to every gene. Manual
119 examination of the HTT peaks in gene bodies shows greater HTT occupancy near the 3' end of the coding
120 region, rather than binding as a sharp peak in a promoter or enhancer, as would be expected if HTT acts as a
121 transcription factor[14]. Genes with this HTT occupancy pattern include canonical markers for SPNs such as
122 *Ppp1r1b* (DARPP32) and *Pde10a* (Fig. 1C-D), which has previously been shown to have altered chromatin
123 conformation in *Htt*$^{Q140/Q140}$ striatum[7].
124

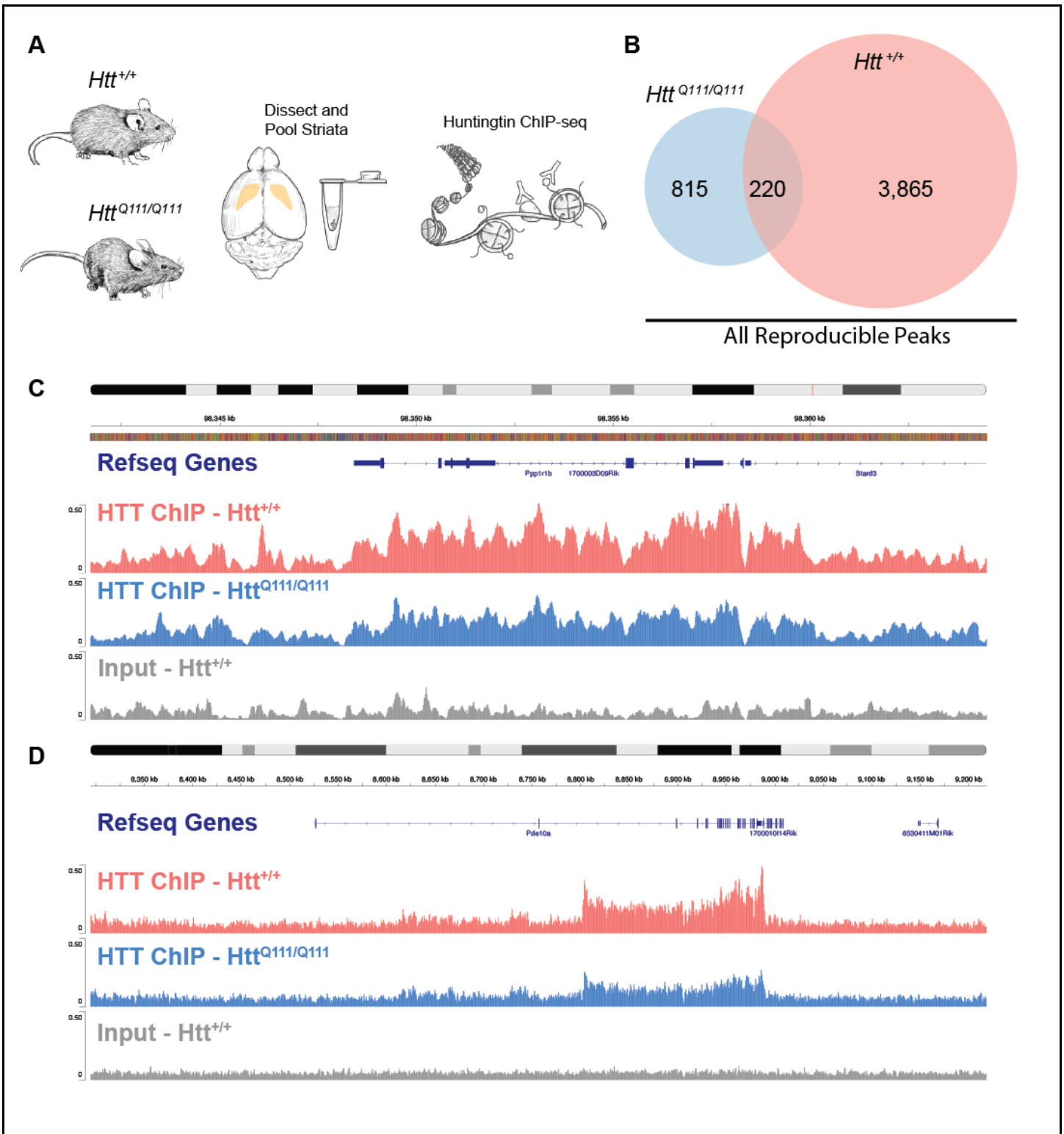

Figure 1: Reproducible huntingtin ChIP-seq peak profiles in 4-month-old *Htt*$^{+/+}$ and *Htt*$^{Q111/Q111}$ mice. A) Schematic of experiment. B) Venn diagram depicting the number *Htt*$^{+/+}$-specific, *Htt*$^{Q111/Q111}$-specific, and shared HTT peaks reproducible at FDR < 0.01 in at least 2 biological replicates from each genotype. C-D) Normalized genomic coverage at representative HTT ChIP-Seq peaks in *Htt*$^{+/+}$ mice (peach) and *Htt*$^{Q111/Q111}$

mice (blue), with *Htt*$^{+/+}$ input control sample (gray). Chromosomal locations and Refseq genes (mouse genome MM10) are indicated. Genes upstream of Pde10a in D) have been omitted for labeling clarity.

Differential Occupancy in *Htt*$^{Q111/Q111}$ mice

Next, we quantified HTT occupancy in *Htt*$^{Q111/Q111}$ vs. wildtype mice using `DiffBind`[25]. We found 244 peaks with significantly lower occupancy in *Htt*$^{Q111/Q111}$ compared to wildtype mice, and 4 peaks with higher occupancy in *Htt*$^{Q111/Q111}$ mice (FDR < 0.1; Fig. 2A; Supplementary Table S3), suggesting a bias towards reduced occupancy in *Htt*$^{Q111/Q111}$ samples. Notably, genes with nearby reduced peak occupancy in *Htt*$^{Q111/Q111}$ striata include important SPN identity genes - many with robust HTT ChIP-seq signal across the coding region - such as *Pde10a* and *Rgs9* (Fig. 2A). To more formally establish the gene sets associated with genes near `DiffBind`-nominated peaks, we assigned peaks to the nearest annotated gene if they overlapped the TSS (-1kb to +100bp), TTS (-100 bp to +1kb), exon, intronic, or intergenic regions (1kb to 1Mb), and conducted enrichment analyses using `enrichR`[26]. Genes near HTT peaks that are reduced in *Htt*$^{Q111/Q111}$ mice relative to *Htt*$^{+/+}$ mice were more likely to be markers of striatal identity, as cataloged by the Mouse Gene Atlas[27] (Fig. 2B; Supplementary Table S4). No such enrichments were found for genes near HTT peaks that are higher in the *Htt*$^{Q111/Q111}$ mice relative to *Htt*$^{+/+}$ mice (data not shown). Next, we investigated enrichments in a collection of 2,579 manually curated HD-relevant transcriptional signatures from the Huntington's Disease Molecular Signatures Database (HDSigDB; https://hdsigdb.hdinhd.org/, 2021 mouse version). Genes near HTT peaks with decreased occupancy in *Htt*$^{Q111/Q111}$ mice were markedly enriched amongst many gene sets from HD mouse studies (Fig. 2C). Most notably, these included genes that are downregulated in the striata of preclinical HD mouse models. These data suggest a pattern of reduced HTT genomic occupancy near SPN identity genes that are transcriptionally downregulated in the striatum across HD model systems.

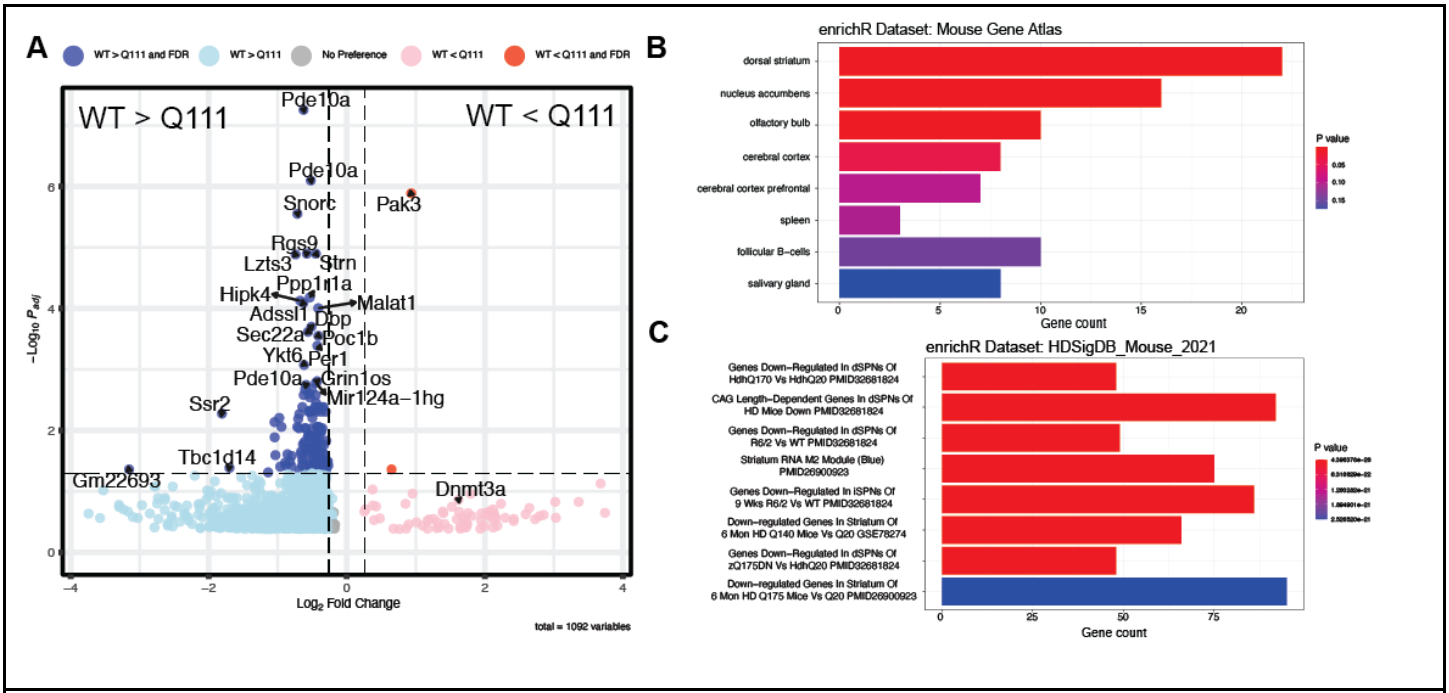

Figure 2: Differential chromatin binding by Huntingtin in *Htt*$^{+/+}$ and *Htt*$^{Q111/Q111}$ mice. A) Volcano plot summarizes the results of the `DiffBind` analysis – the X-axis indicates the fold change and the y-axis the adjusted *p*-value. `DiffBind` peaks for which the FDR is less than 0.05 and/or the absolute fold-change is > 0.26 are identified by the nearest gene symbol. `DiffBind` peaks not matching those criteria are indicated with gray dots. B) 244 genes with reduced peaks in the *Htt*$^{Q111/Q111}$ mice (FDR < 0.1) were examined using `enrichR` for enrichment amongst a number of different mouse tissues. The bar graph indicates the results of these genes amongst mouse tissues with significant enrichments. Only the terms "dorsal striatum" and "nucleus accumbens" meet the stringency threshold $P_{adj} < 0.05$. C) Enrichment of `DiffBind` nominated peaks in HDSigDB gene sets reveals strikingly enriched sets, notably those that include genes which are down-regulated in the striatum of HD mouse models.

Histone Methylation and EZH2 Occupancy in *Htt*$^{Q111/+}$ Mice

To compare HTT occupancy and chromatin states of interest, we generated ChIP-seq of Histone H3 modifications associated with specific chromatin states: trimethylation of lysine 27 (H3K27me3), trimethylation of lysine 9 (H3K9me3), trimethylation of lysine 4 (H3K4me3) and acetylation of lysine 27 (H3K27ac). These marks are associated with active promoters (H3K4me3), active promoters and enhancers (H3K27ac),

151 facultatively repressed promoters and enhancers (H3K27me3), and constitutively repressed regions
152 (H3K9me3). These experiments used striatal tissue from mice of the same age as the *Htt*$^{Q111/Q111}$ animals used
153 in our HTT ChIP-seq experiments described above (N=3/genotype), but utilized heterozygous *Htt*$^{Q111/+}$ mice to
154 enable matched comparisons to published gene expression datasets from heterozygous *Htt*$^{Q111/+}$
155 mice[8,10,21]. After library construction, sequencing, input normalization and peak calling, we identified 17672,
156 25315, 22304, and 27337 reproducible peaks for H3K4me3, H3K27me3, H3K9me3, and H3K27ac,
157 respectively. As expected, H3K4me3 was localized primarily at promoters, H3K27ac and H3K27me3 in
158 enhancers and promoters, and H3K9me3 in more distal regions (Fig. 4A). Using these data, we examined
159 differential methylation, acetylation or occupancy of each dataset in *Htt*$^{Q111/+}$ vs. *Htt*$^{+/+}$ samples. At FDR < 0.1,
160 there were no robust peak differences for H3K9me3, H3K4me3, or H3K27ac, suggesting that any genotypic
161 differences in these marks are subtle. However, we identified 42 H3K27me3 differentially methylated regions
162 (DMRs) at FDR < 0.1 (Supplementary Table S5; Fig. 3A). Notably, 41 of 42 H3K27me3 DMRs (98%) had
163 reduced levels of methylation in *Htt*$^{Q111/+}$ vs. *Htt*$^{+/+}$. At a more lenient p-value (P < 0.05), there were 2018
164 H3K27me3 DMRs, of which 1926 (96%) had reduced methylation in *Htt*$^{Q111/+}$ samples. These results suggest
165 that HD mutations lead to changes in H3K27 trimethylation in the 4-month-old *Htt*$^{Q111/+}$ striatum, including a
166 previously undescribed reduction in H3K27me3 levels in many genomic regions.

167 The reduction of H3K27me3 in *Htt*$^{Q111/+}$ vs. *Htt*$^{+/+}$ striata suggested a possible partial change of PRC2
168 function, the enzymatic complex responsible for "writing" the H3K27me3 mark[20]. We investigated the genes
169 proximal to H3K27me3 DMRs (p-value < 0.05) to gain insight into their potential biological consequences.
170 Functional annotation of H3K27me3 DMRs with `GREAT` [28] and `Genekitr` [29](Fig. 3B; Supplementary Table
171 S6) revealed that negative DMRs in *Htt*$^{Q111/+}$ striata were enriched near genes that impinge on development
172 and morphogenesis (e.g. GO:0001822, Kidney Development, p_{adj} = 4.4e-06), genes involved in synapse
173 formation and stability (e.g. GO:0007416, Synapse Assembly, p_{adj} = 1.4e-10), and genes related to cognitive
174 processes (e.g. GO:0007611, Learning or Memory, p_{adj} = 5.3e-07). Genes associated with decreased
175 H3K27me3 levels were enriched for molecular functions at the synapse (Fig. 3C), including glutamate binding
176 (GO:0016595, p_{adj} = 4.8e-04) and calcium channel activity (GO:0005262, p_{adj} = 9.7e-08). Assessment of
177 negative H3K27me3 DMRs for transcription factor-associated chromosomal localization using `enrichR`
178 indicated enrichment at known PRC2 target genes (i.e. those associated with PRC2 subunits EZH2 and

179 SUZ12; Fig. 3D), many of which are involved in cell fate determination[30]. Notable examples of
180 developmentally important genes near negative H3K27me3 DMRs include the TFs *Sox11* and *Foxp2.*
181 Therefore, mHTT expression in the striatum is associated with reduced H3K27me3 levels in the vicinity of
182 synaptic, as well as developmentally important genes, including transcription factors that are targets of the
183 PRC2 complex. To further explore this, we performed ChIP-seq of EZH2, the enzymatic component of PRC2
184 that is responsible for methylation of H3K27, in the striatum of four-month-old $Htt^{Q111/+}$ and wildtype mice (n = 3
185 / genotype), identifying 12388 reproducible peaks. Interestingly, this analysis revealed no differentially
186 occupied sites (Fig. 3A), suggesting that HD does not alter the localization of the EZH2-containing PRC2
187 complex itself at this age.

188 We next tested the hypothesis that HTT ChIP-seq peaks co-localize with histone modifications and
189 EZH2 (Fig. 3E; Supplementary Table S7). We found a striking overlap between our HTT peaks and EZH2
190 ($\log_2$FC = 3.2; p_{adj} = 3.2e-05), H3K27ac ($\log_2$FC = 2.0; p_{adj} = 3.2e-05), and H3K4me3 ($\log_2$FC = 2.6; p_{adj} = 3.2e-
191 05). We did not observe global overlap between constitutive heterochromatin marked by histone H3 lysine 9
192 trimethylation (H3K9me3; $\log_2$FC = -0.2; p_{adj} = 0.41), and we observed a *depletion* of HTT peaks in H3K27me3
193 peak regions ($\log_2$FC = -1.5; p_{adj} = 3.2e-05). This apparent discrepancy between HTT peaks being enriched in
194 EZH2 regions, but depleted from H3K27me3 peak regions, may indicate differences in the association of HTT
195 with sites of active EZH2-containing PRC2 complexes versus stably methylated H3K27.

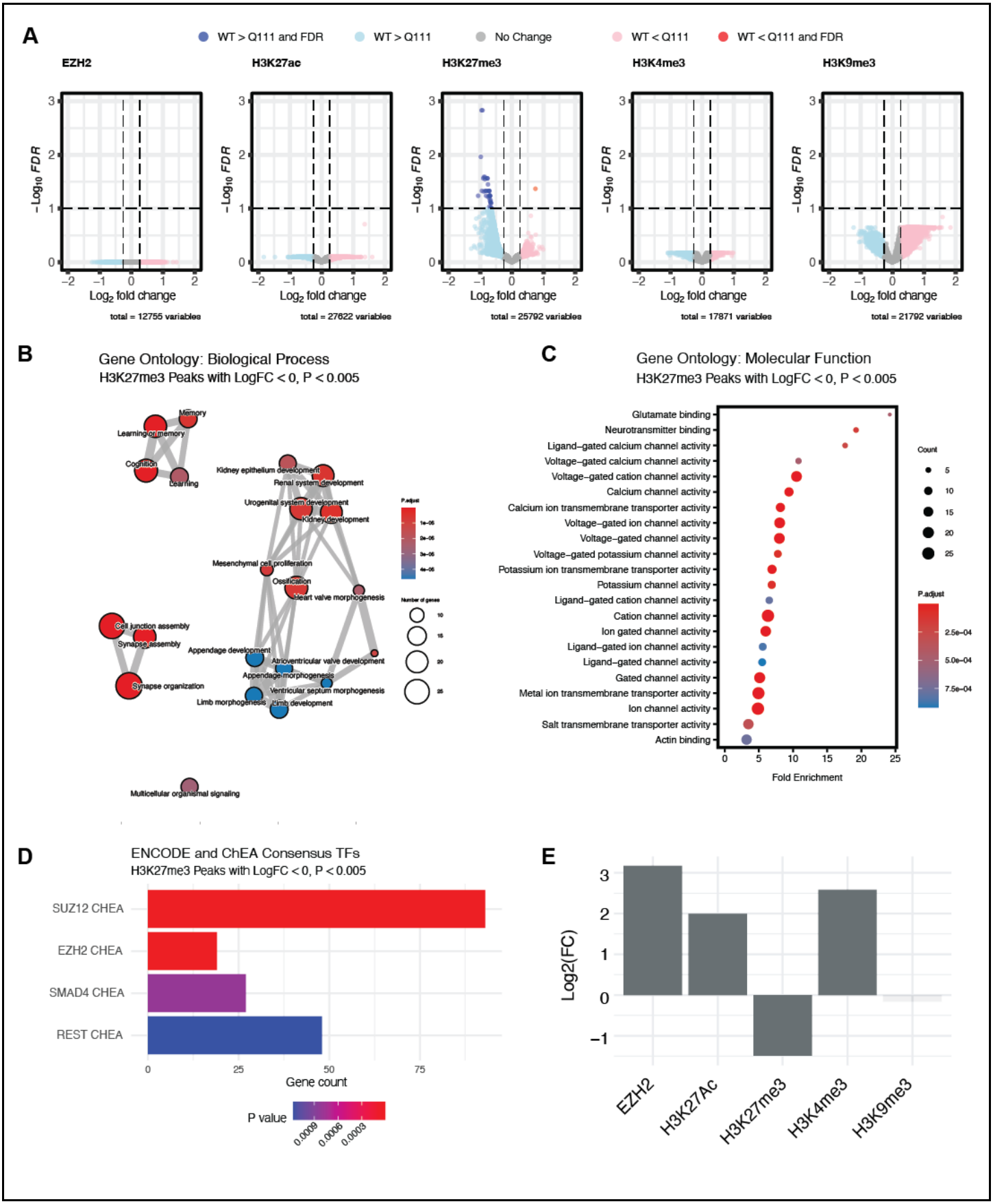
A
WT > Q111 and FDR
WT > Q111
No Change
WT < Q111
WT < Q111 and FDR
EZH2
H3K27ac
H3K27me3
H3K4me3
H3K9me3
−Log10 FDR
Log2 fold change
total = 12755 variables
total = 27622 variables
total = 25792 variables
total = 17871 variables
total = 21792 variables
B
Gene Ontology: Biological Process
H3K27me3 Peaks with LogFC < 0, P < 0.005
Memory
Learning or memory
Cognition
Learning
Kidney epithelium development
Renal system development
Urogenital system development
Kidney development
Mesenchymal cell proliferation
Ossification
Heart valve morphogenesis
Cell junction assembly
Synapse assembly
Appendage development
Atrioventricular valve development
Appendage morphogenesis
Synapse organization
Ventricular septum morphogenesis
Limb morphogenesis
Limb development
Multicellular organismal signaling
P.adjust
Number of genes
C
Gene Ontology: Molecular Function
H3K27me3 Peaks with LogFC < 0, P < 0.005
Glutamate binding
Neurotransmitter binding
Ligand−gated calcium channel activity
Voltage−gated calcium channel activity
Voltage−gated cation channel activity
Calcium channel activity
Calcium ion transmembrane transporter activity
Voltage−gated ion channel activity
Voltage−gated channel activity
Voltage−gated potassium channel activity
Potassium ion transmembrane transporter activity
Potassium channel activity
Ligand−gated cation channel activity
Cation channel activity
Ion gated channel activity
Ligand−gated ion channel activity
Ligand−gated channel activity
Gated channel activity
Metal ion transmembrane transporter activity
Ion channel activity
Salt transmembrane transporter activity
Actin binding
Fold Enrichment
Count
P.adjust
D
ENCODE and ChEA Consensus TFs
H3K27me3 Peaks with LogFC < 0, P < 0.005
SUZ12 CHEA
EZH2 CHEA
SMAD4 CHEA
REST CHEA
Gene count
P value
E
Log2(FC)
EZH2
H3K27Ac
H3K27me3
H3K4me3
H3K9me3

Figure 3. ChIP-seq analysis reveals early changes in H3K27me3 near developmentally important genes in *Htt*$^{Q111/+}$ mice. A: Volcano plots summarizing differential histone modifications for H3K27me3, H3K9me3 and H3K4me3 and differential occupancy for EZH2 in striatal tissue from four-month-old in *Htt*$^{Q111/+}$ vs. *Htt*$^{+/+}$ mice. The x-axis indicates the $\log_2$FC and the y-axis indicates the -$\log_{10}$(p-value) for the comparison of peak read depth between genotypes. Regions with greater levels or occupancy in the *Htt*$^{+/+}$ mice are shown in blue, regions with greater levels or occupancy in the *Htt*$^{Q111/+}$ mice are shown in pink/red. The dashed horizontal line indicates an FDR of 0.1 and vertical lines are Log_2FC = +/-0.26. B) Network depiction of Gene Ontology Biological Processes enrichment near differentially methylated regions with reduced H3K27me3 in *Htt*$^{Q111/+}$ mice. C) Gene Ontology Molecular Function enrichment near differentially methylated regions with reduced H3K27me3 in *Htt*$^{Q111/+}$ mice. D) Enrichment of 495 genes in nominally differentially methylated regions with reduced H3K27me3 in *Htt*$^{Q111/+}$ mice (unadjusted $p < 0.005$) amongst a consensus transcription factor/target gene databases (i.e. ENCODE and ChEA Consensus TFs from the `enrichR` package). Robustly enriched transcription factor lists include: SUZ12 CHEA (93/1,684; p_{adj} = 8.3e13; EZH2 CHEA (19/237; p_{adj} = 2.0e04); SMAD4 CHEA (27/584; p_{adj} = 2.6E02); REST CHEA (48/1,280; p_{adj} = 2.8e02). E) Enrichment of EZH2 and indicated chromatin mark ChIP-seq peaks (MACS FDR < 0.05) in huntingtin ChIP-seq peak regions. Y-axis indicates the log-transformed fold change (enrichment or depletion) in the number of overlapping base pairs compared to the average from 100,000 re-sampling permutations of genomic coordinates. Plotting color indicates the p-value, derived from these same permutations.

196

197 # HTT Binds Specific Chromatin Domains

198 To explore a role for HTT in gene regulation, we compared the locations of all 9624 HTT peaks we
199 observed to known genomic features using the `ChIPseeker` Bioconductor package[24]. HTT's occupied
200 genomic regions differed substantially compared to the other marks (Fig. 4A), with a notable enrichment within
201 introns, consistent with HTT's consistent coverage over coding regions of target genes. Considering the
202 abundance of all peaks relative to the transcriptional start site (TSS), huntingtin peaks were substantially less
203 enriched near the TSS compared to marks canonically associated with active transcription and open chromatin

204 (H3K4me3, H3K27ac) and those of EZH2, which also occupied regions upstream of the TSS of target genes,
205 and less enriched in distal intergenic regions than H3K9me3 (Fig. 4B). HTT peaks had a distinct profile relative
206 to the TSS compared to each of the other mark examined (Fig. 4B), and of the marks surveyed here were the
207 only ones with increased signal near the transcription termination site (TTS; Fig. 4C).

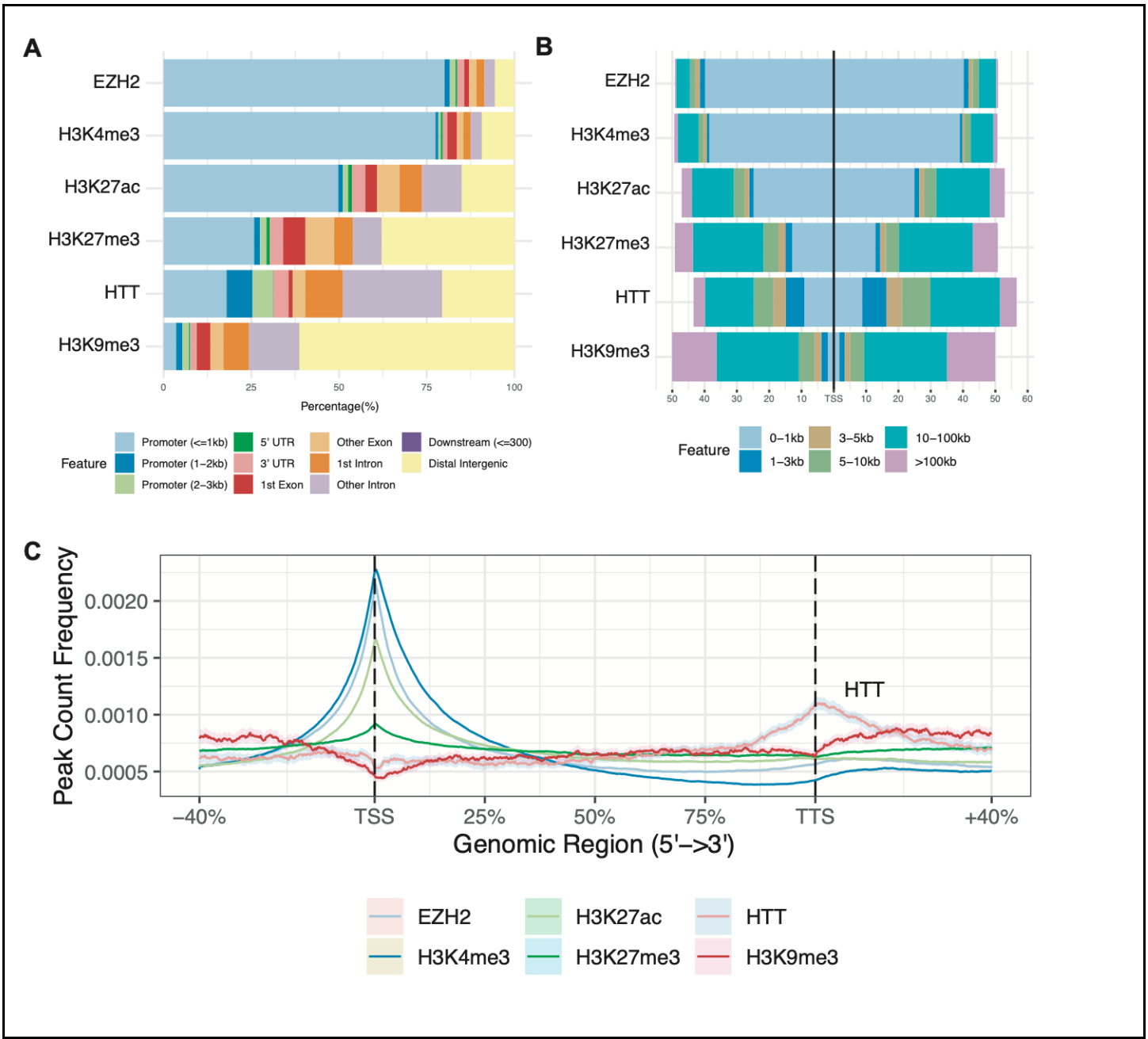

Figure 4. Huntingtin peaks occupy specific chromatin functional regions. A) Summary of genomic regions occupied by huntingtin and other histone mark / EHZ2 occupancy peak sets generated in this study. The percentage of peaks for each dataset are indicated on each vertical line, with boxes indicating the percentage of that marks found in each of the categories indicated. B) Localization of peaks for the indicated

chromatin-associated protein at binned distanced from an averaged transcriptional start site (TSS). C) Peak count frequencies of genic ChIP-seq peaks across the normalized transcript length of all mouse transcripts. The average peak count is indicated via the black bar, from 5' (left) to 3' (right). Genomic regions are indicated as percentages, with 100% spanning from the TSS to the transcriptional termination site (TTS). Shading indicates bootstrapped 95% confidence intervals calculated with resampling (`ChIPSeeker` package).

208

209 ## HTT occupancy predicts effects gene expression in HD

210 The selective enrichment of HTT binding within regions of chromatin bearing marks associated with
211 active transcription (H3K4me3 and H3K27ac; Fig. 1E), and its depletion from a mark associated with
212 repressive transcription (H3K27me3; *ibid*) raised the possibility that HTT may directly contribute to HD-related
213 changes in gene expression. We mapped potential HTT target genes whose TSSs were located within +/- 20
214 kb of a HTT ChIP peak. Assigning regulatory elements to their target genes is inevitably inexact, but previous
215 work has shown that summing the regulatory elements within 20 kb of a TSS optimizes sensitivity and
216 specificity for detecting gene regulatory interactions[31]. Given HTT's striking occupancy at specific genes (e.g.
217 Fig. 1C-D, Fig. 2), we considered whether it might more generally occupy regions near genes with disease-
218 relevant changes in gene expression. We first considered the simplest category of interest: genes that are up-
219 or down-regulated in the striatum of HD model mice, with a focus on the $Htt^{Q111/+}$ striatum at 6 months of age,
220 taken from a larger allelic series study[10]. We find enrichment of HTT peaks (irrespective of peak category, or
221 "All Reproducible") near genes that are downregulated in the striatum of 6-month-old $Htt^{Q111/+}$ mice (Fig. 5A;
222 $\log_2$FC = 0.73, p_{adj} = 1.4e-30) and depleted near genes that are up-regulated (Fig. 5A; $\log_2$FC = -0.33, p_{adj} =
223 5.3e-05). Expanding this analysis to differentially expressed genes in other mouse lines and timepoints from
224 the allelic series study reinforced our observation that HTT-occupied chromatin peaks are more likely to be
225 associated with down-regulated genes than up-regulated genes (Fig. 5B, Supplementary Table S8).
226 We next examined the enrichment of our HTT peaks amongst all manually curated gene sets cataloged
227 in the HDSigDB database (Fig. 5C, Supplementary Table S9). As with our `DiffBind`-nominated peaks with

228 differential binding in *Htt*$^{Q111/Q111}$ versus *Htt*$^{+/+}$ mice (Fig. 2), this analysis revealed a striking enrichment
229 amongst genes that are dysregulated in a number of studies, and particularly in striatal genes that are down-
230 regulated in HD (e.g. Fig. 5B). A particularly notable gene set is the "Striatum RNA M2 Module (blue)" from an
231 exhaustive molecular network characterization of an allelic series of HD knock-in mice[10]. This module of
232 genes is notable for being tightly correlated with CAG length and age in the striatum of mHTT-expressing mice
233 and contains many striatal identity genes. This suggests that our HTT peaks are markedly enriched amongst
234 striatum-expressed genes, including SPN identity genes which are down-regulated in HD. Given PRC2's role
235 in regulating cell-specific gene expression and described interactions with HTT[17], we specifically focused on
236 PRC2-relevant gene sets in HDSigDB. Our shared HTT peaks, those found in both wildtype and Q111/Q111
237 mice, were strikingly enriched in bivalent genes whose expression is increased at 3- (Fig. 5C; Odds ratio =
238 16.7, FDR = 7.6e-05) and 6-months of age (Fig. 5C; Odds ratio = 6.2, FDR = 3.6e-03) in the striatum of mice
239 lacking PRC2 expression in SPNs (*Ezh1*$^{-/-}$;*Ezh2*$^{-/-}$)[18]. This suggests that our peaks are near genes that are
240 both down-regulated in HD, *and* up-regulated in the context of PRC2 knockout, supporting the hypothesis that
241 HTT binding at a small set of bivalent genes may play an important role in gene dysregulation in HD.
242 Consistent with our own data (Fig. 3D), revealing a depletion of HTT peaks in H3K27me3 regions, our mutant-
243 specific HTT peaks were depleted near H3K27me3-enriched genes in purified SPNs (Fig. 5C; Odds ratio =
244 16.7, FDR = 7.6e-05)[18] .

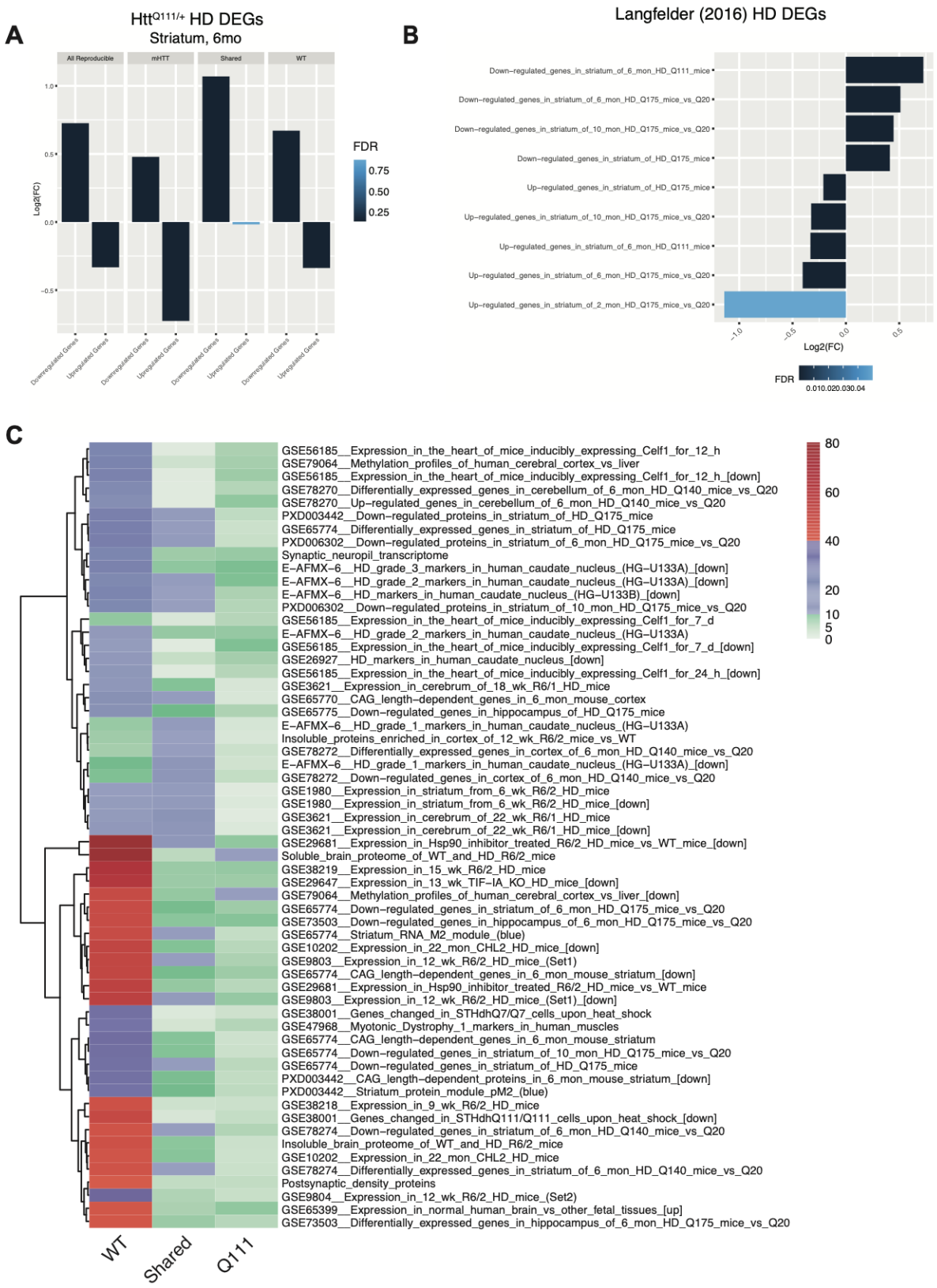

Figure 5. Genotype-specific HTT occupancy in genomic regions surrounding HD DEGs and other CAG-sensitive gene sets of interest. A-B) Enrichment or depletion of HTT ChIP-seq peaks in the regions

+/- 20 kb from the transcription start sites of up- and down-regulated differentially expressed genes (DEGs) in the striatum of knock-in mouse models of HD mutations, based on RNA-seq from [10,46]. Y-axis indicates fold enrichment of base pair overlap compared to the average from 100,000 re-sampling permutations. C) Heatmap showing HDSigDB gene sets enriched in the regions +/- 20 kb of WT-specific, Q111-specific, and Shared HTT ChIP-seq peaks. The plotting color indicates the -$\log_{10}$(p-value) for the strength of the enrichment, based on 100,000 re-sampling permutations. Rows are ordered by hierarchical clustering, based on p-values.

245

246 Correlations Between HTT Binding and Epigenetic Features Near HD DEGs

247 We hypothesized that the negative correlation between HTT occupancy and HD-related gene
248 expression may be mediated by PRC2 and histone modifications. To investigate this, we integrated our data
249 on HTT occupancy, histone modifications, and transcription, focusing on the genomic regions proximal to
250 DEGs in 6-month-old *Htt*$^{Q111/+}$ versus *Htt*$^{Q20/+}$ mice (Fig. 6A-C; Table S8 [10]). We defined intervals of interest
251 +/- 20 kb of the TSS of each HD DEG and calculated the fold change in *Htt*$^{Q111/Q111}$ vs. *Htt*$^{+/+}$ mice for HTT,
252 H3K27me3, H3K4me3, and EZH2 occupancy within the same interval. Consistent with our hypothesis, the fold
253 changes in H3K27me3 were constitutively lower and negatively correlated with HTT occupancy near genes
254 differentially expressed in HD (Fig 6B; Spearman's rho = -0.22; p = 1.3e-3). This suggests that *Htt*$^{Q111/+}$ mice
255 have generally lower H3K27me3 levels near HD DEGs, and that increased HTT binding in a region is
256 associated with reduced H3K27me3 in the same interval. Conversely, in those same regions we observe
257 constitutively higher, and positively correlated, relationships across genotypes between HTT binding and
258 H3K4me3 (Fig 6C; Spearman's rho = 0.27; p < 1e-300) and EZH2 (Fig. 6A; Spearman's rho = 0.14; p = 1.5e-
259 2). That is, in *Htt*$^{Q111/+}$ mice, near HD DEGs, levels of EZH2 occupancy and H3K4me3 were generally higher,
260 with increased HTT binding in that region associated with more EHZ2 occupancy and higher H3K4me3 levels
261 in that same interval. Conversely, levels of H3K27me3 near HD DEGs were lower in Htt$^{Q111/+}$ mice, and greater
262 local HTT binding predicts lower H3K27me3. Importantly, these relationships appeared to hold true both for
263 up- and down-regulated genes in *Htt*$^{Q111/+}$ mice. Thus, concordant changes in PRC2 localization and histone

methylation/demethylation may coincide with alterations in HTT occupancy in these regions in both *Htt*$^{Q111/+}$ and *Htt*$^{+/+}$ mice.

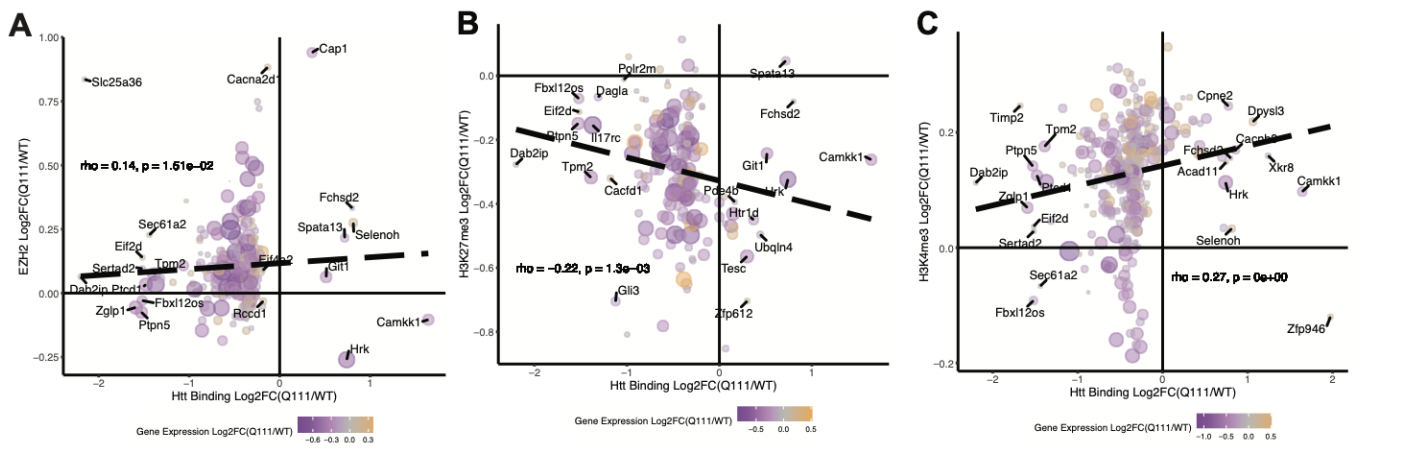

Figure 6. Increased HTT occupancy is negatively associated with H3K27me3 and positively associated with H3K4me3, near genes that are dysregulated in HD. Each plot indicates the fold change of HTT occupancy in *Htt*$^{Q111/Q111}$ vs. *Htt*$^{+/+}$ mice (x-axis) compared to the fold change in the same regions for EZH2 (A), H3K27me3 (B), and H3K4me3 (C) on the y-axis. Analysis is restricted to 263 HTT peaks located +/- 20 kb from the TSSs of genes that are significantly up- or down-regulated in the striatum of six-month-old knock-in mouse models of HD mutations. Each point represents a single HTT ChIP-seq peak. Point color indicates the fold change in gene expression in the striatum of HD knock-in mice (up = yellow; down = purple), and point size corresponds to the p-value for differential expression.

Discussion

This study was motivated by the question of whether transcriptional dysregulation in Huntington's disease could occur due to interactions between HTT and chromatin. Previously, we investigated whether specific transcription factors demonstrated differential genomic occupancy and compared this with gene expression changes in *Htt*$^{Q111/+}$ mice, finding that the transcription factor SMAD3 demonstrated differential binding between wildtype and mutant mouse brain tissue[10,32]. This finding led us to ask what role the HTT protein itself might play with regards to codified chromatin interactions.

274 ChIP-seq of the HTT protein reveals thousands of robust and reproducible sites of HTT genomic
275 occupancy in the mouse striatum, the brain region most vulnerable to HD pathology and in which the most
276 pronounced transcriptional dysregulation occurs. Many HTT peaks are enriched across the coding sequence of
277 genes of particular interest in HD, with a surprising enrichment near the 3' end of many transcripts. We further
278 observed, for the first time, a reduction in the levels of H3K27me3 in the striatum of young *Htt*$^{Q111/+}$ mice,
279 suggesting these changes represent a very early stage of chromatin alterations in the most vulnerable brain
280 region in HD, which experiences the greatest burden of transcriptional changes in HD. HTT peaks are enriched
281 near genes that are down-regulated in HD, and depleted near genes that are up-regulated, supporting a link
282 between these HTT:chromatin interactions and bi-directional gene expression changes in HD. An integrated
283 analysis of HTT binding and histone marks suggests that local HTT binding near HD DEGs is associated with
284 increased H3K4me3 and EZH2 binding, and reduced H3K27me3 levels.

285 HTT physically interacts with transcriptional regulatory proteins such as p53 and CREB-binding
286 protein[33]. In addition, previous ChIP-qPCR experiments with HTT antibodies suggested occupancy in
287 promoter regions of specific genes[14]. With the improved resolution of genome-wide ChIP-seq, we observed
288 thousands of robust HTT:chromatin interactions in a specific subset of genes. However, these HTT peaks are
289 not primarily localized to the promoters. Instead, distributions of HTT occupancy across genic regions were
290 more reminiscent of marks such as H3K36me3[34,35] and RNAPII Ser2[36,37] that are associated with
291 transcriptional elongation and enriched at the 3' end of the gene, a pattern distinct from active marks such as
292 H3K4me3 that are more strongly associated with TSSs[38,39]. Thus, both the gene identity and pattern of HTT
293 binding in those genes argues for a specific, selective, role for HTT-chromatin interactions. This argument is
294 strengthened by the fact that the specific genes with robust HTT occupancy in the striatal tissue we profiled are
295 enriched for SPN identity genes which we [19], and others[10,19], have found to be strikingly downregulated in
296 HD.

297 Many genes with HTT peaks identified in our study are targets of the PRC2 complex, a critical regulator
298 of cell identity via regulation of the H3K27me3 mark near genes important for cell-fate commitment[20],
299 including in SPNs of the striatum[18], the most vulnerable brain region to HD pathology[2,18]. Direct
300 interactions between HTT and the PRC2 complex have been described, and HTT has been proposed to
301 directly enhance the activity of the enzymatic activity of the PRC2 complex[17]. The enrichment of HTT within

302 well-annotated PRC2 target genes supports a role for HTT in regulating their expression, however, in the
303 aggregate, the occupancy patterns of EZH2 and HTT are quite distinct (Fig. 4A-C). And while, genome-wide,
304 we observe robust overlap between HTT and EZH2 peaks, we observe a *depletion* of HTT in H3K27me3 peak
305 regions (Fig. 3D), suggesting HTT is unlikely to occupy all chromatin-bound PRC2 complexes, nor remain
306 associated with facultative heterochromatin, once formed. Given its role in scaffolding functional protein-protein
307 interactions[17,40], and dynamic shuttling between the nucleus and cytoplasm[41], we hypothesize that HTT
308 may play a role in regulating the balance between active and repressed chromatin at select PRC2 target
309 genes.

310 Several potential mechanisms for HTT's involvement in transcriptional regulation via the PRC2 complex
311 deserve attention in future studies. A functionally important role for interactions between HTT and the
312 repressor element 1 silencing transcription factor (REST), which plays important roles in repressing neuronal
313 gene expression in non-neuronal cells, have been described[42]. Namely, HTT and REST bind, and HTT aids
314 in confining REST to the cytoplasm, thereby preventing aberrant expression of REST target genes in non-
315 neuronal cells. Expression of mHTT results in the aberrant accumulation of REST in the nucleus, and
316 consequential dysregulation of REST-mediated signaling. With this background, we were intrigued with our
317 results demonstrating that regions with lower H3K27me3 in the striata of *Htt*$^{Q111/+}$ mice are enriched in both
318 PRC2 and REST target genes (Fig. 3D), especially considering data suggesting that REST may be involved in
319 targeting PRC2 to specific loci[42,43]. Recently, a new pathway for regulation of PRC2 function via cytoplasmic
320 retention of embryonic ectoderm development (EED), a PRC2 subunit critical for formation of the complete
321 trimeric structure, has been described[44]. In post-mitotic myotubes, a short cytoplasmic form of PRC2 subunit
322 EZH1 (EZH1β) sequesters EED in the cytoplasm, preventing formation of the PRC2 complex at target genes in
323 the nucleus. Future work focused on understanding whether HTT plays a role in the regulation of PRC2
324 signaling via cytoplasmic sequestration of PRC2 subunits may be a fruitful area of investigation.

325 We complemented our HTT ChIP-seq findings with ChIP-seq of histone modifications and EZH2
326 binding, which revealed reductions in H3K27me3 in the striatum of young *Htt*$^{Q111/+}$ mice, similar to those seen
327 in *Htt*$^{Q140/+}$ mice[7] and particularly near important striatal cell identity genes (e.g. *Pde10a*). Our differential
328 acetylation data do not recapitulate large-scale genotype-dependent changes in H3K27ac previously seen in
329 HD mouse model striatum, which could be due to our use of bulk tissue versus fluorescence-activated nuclear

330 sorted neurons[7]. Further, while we do see association of HTT peaks with H3K27ac (Fig. 4E), HTT shows less
331 association than with EZH2 and H3K4me3, suggesting that HTT is likely not localized to super-enhancers but
332 instead to gene bodies (Fig. 3A). The observed reduction in H3K27me3 in *Htt*$^{Q111/+}$ mice is consistent with a
333 hypothesis of PRC2 complex dysfunction and/or trafficking disruption occurring at the earliest stages of
334 progression in this model, though other chromatin modifiers could also play roles. The identified lower levels of
335 H3K27me3 seen in heterozygous polyQ HTT-expressing striatum and lack of changes in EZH2 occupancy in
336 particular may implicate H3K27-targeted histone demethylases such as KDM6A/UTX in epigenetic changes
337 observed in HD[45]. While correlational, our integrated analysis of HTT, EZH2 binding, and histone marks
338 suggests that increased HTT binding near HD DEGs in *Htt*$^{Q111/+}$ mice predicts increased H3K4me3 and EZH2
339 binding, with reduced H3K27me3 at these same loci. We believe detailed mechanistic experiments focused on
340 elucidating the pathways linking these events could provide important new insights into HTT's role in
341 transcriptional dysregulation in HD.

342 This study has several important limitations. Like all ChIP-seq studies, peak detection is sensitive to
343 background noise, antibody cross-reactivity, and other sources of bias. We have tried to control for this by
344 using a relatively large number of technical and biological replicates. Another consideration is the reliance on
345 antibodies, which limits us to establishing chromatin regions associated with specific epitopes of HTT. Future
346 work using phospho-specific antibodies, and other dynamic epitopes is likely to nominate additional HTT-
347 chromatin interactions, which are of great interest. Functional enrichment analyses of our diffbind results from
348 wildype HTT versus mHTT rely on gene assignment that may be biased towards longer genes, propagating
349 these biases through the enrichment tools. This is likely less of an issue for HTT, since many of its peaks are
350 directly over gene bodies, but highlights that predicting the potential regulatory functions of distal peaks is
351 difficult. Finally, our ChIP-seq experiments relied on bulk striatal tissue, whereas single-nuclei RNA
352 sequencing has indicated bidirectional effects of HD mutations across cell types, especially for PRC2
353 targets[19]. Emerging techniques enabling ChIP-seq of single cells and sorted cell populations[19,46] should
354 enable additional refinements of the findings presented here.

355 While ChIP-on-chip has been performed to identify HTT binding sites at promoter sequences[14], this
356 work provides the first genome-wide map of HTT-chromatin interactions and has identified key changes in
357 these interactions due to HD mutations. It suggests that aberrant de-repression of CAG-sensitive genes in HD

358 samples–including cell identity genes–may be due to molecular interactions of HTT and chromatin. We find
359 that altered HTT-chromatin occupancy is accompanied by novel histone modification changes – notably,
360 reductions in H3K27me3 – in the *Htt*$^{Q111/+}$ striata, which are associated with genotype-selective HTT occupancy
361 in the same regions. In fact, the strength of HTT occupancy predicts increased H3K4me3 and EZH2
362 occupancy, and reductions in H3K27me3, consistent with a model in which HTT plays a functional role in
363 regulating PRC2 activity, perhaps by helping recruit PRC2 to specific loci.
364

365 Conclusions

366 Collectively, our data support a model of pathogenesis in which perturbation of normal HTT chromatin
367 regulatory functions precipitates transcriptional dysregulation in HD, leading to epigenetic changes and loss of
368 cell type-specific gene expression.
369

370 Materials and Methods

371 **Mouse Breeding, Genotyping, and microdissection**. The B6.*Htt*^{Q111} mice (Strain 003456; JAX) used for the
372 ChIP-seq study have a targeted mutation replacing mouse *Htt* exon 1 with the corresponding portion of human
373 *HTT* exon 1, including an expanded CAG tract. The targeted *Htt* allele was placed from the CD-1 background
374 onto the C57BL/6J genetic background by selective backcrossing for more than 10 generations to the
375 C57BL/6J strain at Jackson laboratories. Cohorts of homozygote, heterozygote and wildtype littermate mice
376 were generated by crossing B6.*Htt*$^{Q111/+}$ and B6.*Htt*$^{+/+}$ mice. Male mice were sacrificed at four months of age via
377 a sodium pentobarbital based euthanasia solution (Fatal Plus, Henry Schein). Brain tissues were snap frozen
378 in liquid nitrogen and stored in -80°C until ChIP was performed. Experiments were performed following NIH
379 animal care guidelines and approved by Western Washington University's Institutional Animal Care and Use
380 Committee under protocols 14-005 and 16-011.
381

382 **Huntingtin knockdown in cortex.** Four-month-old male mice underwent unilateral intracerebroventricular
383 injection of 500ug pan-huntingtin antisense oligonucleotide (Ionis #444652) or received no treatment. Tissue
384 was collected as above at four weeks post-injection; a time shown to have maximal HTT reduction in BACHD
385 mice[47]. Cortical tissue contralateral to the injection was used to assess HTT knockdown by western blot as
386 described[48], and ipsilateral tissue was used for ChIP as performed below.
387
388 **HTT ChIP-seq.** We prepared replicate (n = 3) ChIP samples using an anti-huntingtin antibody from four-month-
389 old male $Htt^{Q111/Q111}$ and age-matched $Htt^{+/+}$ mice. For each ChIP preparation, chromatin DNA was prepared
390 using the combined striatal tissue from both hemispheres of three mice. Preliminary experiments suggested
391 that this was the minimal amount of material required to provide enough material for multiple IPs. Striata were
392 transferred to a glass Dounce on ice and homogenized in cold phosphate-buffered saline with protease
393 inhibitors. For ASO-treated cortices, two cortices were pooled for each replicate (n = 1). High-resolution X-
394 ChIP-seq was performed as previously described [49], with slight modifications[32]. IPs were performed using
395 Abcam anti-huntingtin EPR5526 (#ab109115). ChIP-seq library preparation and sequencing reactions were
396 conducted at GENEWIZ, Inc. (South Plainfield, NJ, USA). Sequencing was performed on an Illumina HiSeq
397 4000 using 2x150 Paired End (PE) configuration. Sequencing reads were aligned to the mouse genome
398 (mm10) using HISAT2. Peak-calling was then performed with MACS2.2, scaling to the size of the input control
399 library. The final set of reproducible peaks was obtained using the `dba` function in the `DiffBind` R
400 package[25], retaining peaks that were reproducible at FDR < 0.01 in at least two samples and excluding
401 artifactual blacklist regions from ENCODE. Sequence reads have been deposited in gene expression omnibus,
402 accession GSE150750.
403
404 **Histone mark and EZH2 ChIP-seq.** Fresh frozen striatal tissue from five male four-month-old $Htt^{Q111/+}$ and
405 age-matched $Htt^{+/+}$ mice were pooled per replicate for n = 3 samples. Further processing was performed at
406 Active Motif (Carlsbad, CA). Tissue was fixed in 1% formaldehyde, lysed, and disrupted with a Dounce
407 homogenizer. DNA was sonicated to an average fragment length of 300-500bp, and 25ug chromatin plus
408 200ng *Drosophila* spike-in chromatin was incubated with antibody targeting EZH2, H3K27me3 or H3K4me3
409 (Active Motif catalog numbers 39901, 39155 and 399159, respectively). Antibody against H2Av was also

410 present in the reaction to ensure efficient pull-down of the spike-in chromatin. Complexes were captured using
411 protein A agarose beads (Invitrogen). Illumina sequencing libraries were prepared from ChIP and Input DNA by
412 end-polishing, dA-addition, and adaptor ligation. Libraries were quantified and sequenced on Illumina's
413 NextSeq 500 (75nt single end reads).
414
415 **Analysis of striatal HTT ChIP-seq data.** For the primary striatal HTT ChIP-seq dataset, sequencing reads
416 were aligned to the mouse genome (mm10) using `bowtie2` [50]. Peak-calling on each sample was performed
417 with MACS v2.1 [23]**,** scaling each library to the size of the input DNA sequence library to improve
418 comparability between samples. We retained peak regions with a MACS p-value < 0.001. Filtered peak calls
419 were concatenated across all $Htt^{+/+}$ and $Htt^{Q111/Q111}$ samples to produce a combined set of peak calls and
420 removed peaks overlapping artifactual blacklisted regions of the genome[51].
421
422 **Analysis of cortex HTT ChIP-seq data.** Sequencing reads were aligned to the mouse genome (mm10) using
423 HISAT2. Aligned reads from the four ChIP libraries were down-sampled to the size of the smallest sequencing
424 library using `samtools` view -s[52]. Aligned reads from the input genomic DNA of all four samples were
425 merged into a single control BAM file. Peak-calling was then performed with MACS2.2, scaling to the size of
426 the input control library. The final set of reproducible peaks was obtained using the `dba` function in the
427 `DiffBind` R package, retaining peaks that were reproducible at FDR < 0.01 in at least two samples and
428 excluding artifactual blacklist regions from ENCODE [38]. We then used `dba.count` to count the reads in
429 each peak region from each ChIP sample and from the control sample. Next, a generalized linear model was
430 fit, using the `dba.analyze` DESeq2 wrapper, and we performed log-ratio tests to estimate effects of ASO
431 treatment on HTT occupancy in each peak region. Genotype was treated as a blocking factor. Control read
432 counts were subtracted for each site in each sample before fitting the model. This experiment was
433 underpowered to detect statistically significant changes in occupancy at individual peak regions. Therefore, our
434 primary test was for global depletion of HTT occupancy in ASO-treated mice across peak regions. For this
435 purpose, we computed one-sided binomial tests with `binom.test`, comparing the number of peaks with
436 increased vs. decreased occupancy.
437

438 **Analysis of histone mark and EZH2 ChIP-seq.** Reads were aligned consecutively to the mouse (mm10) and
439 *Drosophila* (dm3) genomes using the BWA algorithm (default settings). The number of mouse alignments used
440 in the analysis was scaled to the number of *Drosophila* spike-in alignments [53]. Peak-calling was performed
441 with MACS v2.1. We selected peaks that were reproducibly identified in at least two samples of the same
442 genotype. For analyses of differential occupancy, reads mapped to each peak region were normalized to total
443 library size. Generalized linear models and log-ratio tests were fit with `edgeR[54]` to identify differentially
444 methylated regions.
445
446 **Enrichment of peaks in genomic regions and gene sets.** Over-representation of HTT peaks in chromatin
447 states, genomic regions marked by histone modifications, and gene sets were calculated using the Genomic
448 Association Tester (GAT; [55]). GAT calculates the number of base pairs overlapping between two genomic
449 annotations and estimates its fold enrichment and significance based on re-sampling permutations within the
450 mappable genome. Results described in this manuscript are based on 100,000 re-sampling permutations.
451 Accession numbers for comparison datasets are shown in the Key Resources Table. For ChromHMM and
452 ChIP-seq comparison datasets, we downloaded published tables of peak regions from the ENCODE portal or
453 from the Gene Expression Omnibus. Similarly, for analyses of gene sets, we downloaded gene lists from
454 HDSigDB (https://www.hdinhd.org/2018/05/22/hdsigdb/), and we defined the regions of interest as +/- 20 kb of
455 the canonical TSSs of the genes in each set.
456
457 **Code and Data Availability.** Code used in the analysis of ChIP-seq data is publicly available:
458 https://github.com/seth-ament/ament-carroll-collab. ChIP-seq data have been deposited in the Gene
459 Expression Omnibus (GSE150750). Processed ChIP-seq data, including peak locations (BED files) and
460 genomic coverage (bigWig files), have been deposited in the Neuroscience Multi-Omic Archive (NemO
461 Archive), where we have created a TrackHub, suitable for viewing in the UCSC Genome Browser:
462 http://data.nemoarchive.org/other/grant/sament/sament/htt-chipseq/.
463

Acknowledgements

We thank Steven Henikoff, Peter Skene, and Christine Codomo for guidance on X-ChIP-seq protocol optimization, as well as the members of the Carroll lab for discussion regarding the findings and manuscript preparation. This work was supported by the CHDI Foundation (J.B.C., S.A.A.), a Huntington Society of Canada New Pathways grant (J.B.C.), and a National Science Foundation Graduate Research Fellowship to JRP.

Author Contributions

Conceptualization: JRP, JPC, LEH, NDP, SAA and JBC. Supervision: LEH, NDP, SAA and JBC. Investigation: JPC, DEB, HRP, RMB, SRC. Data Curation, Formal Analysis, and Visualization: ACS, JBC, JPC, and SAA. Funding Acquisition: JBC, SAA. Writing – Original Draft: JBC, JPC, SAA. All authors reviewed and approved the final manuscript.

Conflict of Interests

JBC has received research support from Ionis Pharmaceuticals, Wave Life Sciences, Triplet Therapeutics and consulting fees from Skyhawk Therapeutics and Guidepoint. None of these companies had any role in the design or interpretations of these experiments. Other authors report no conflicts.

Supplementary Information Titles and Legends

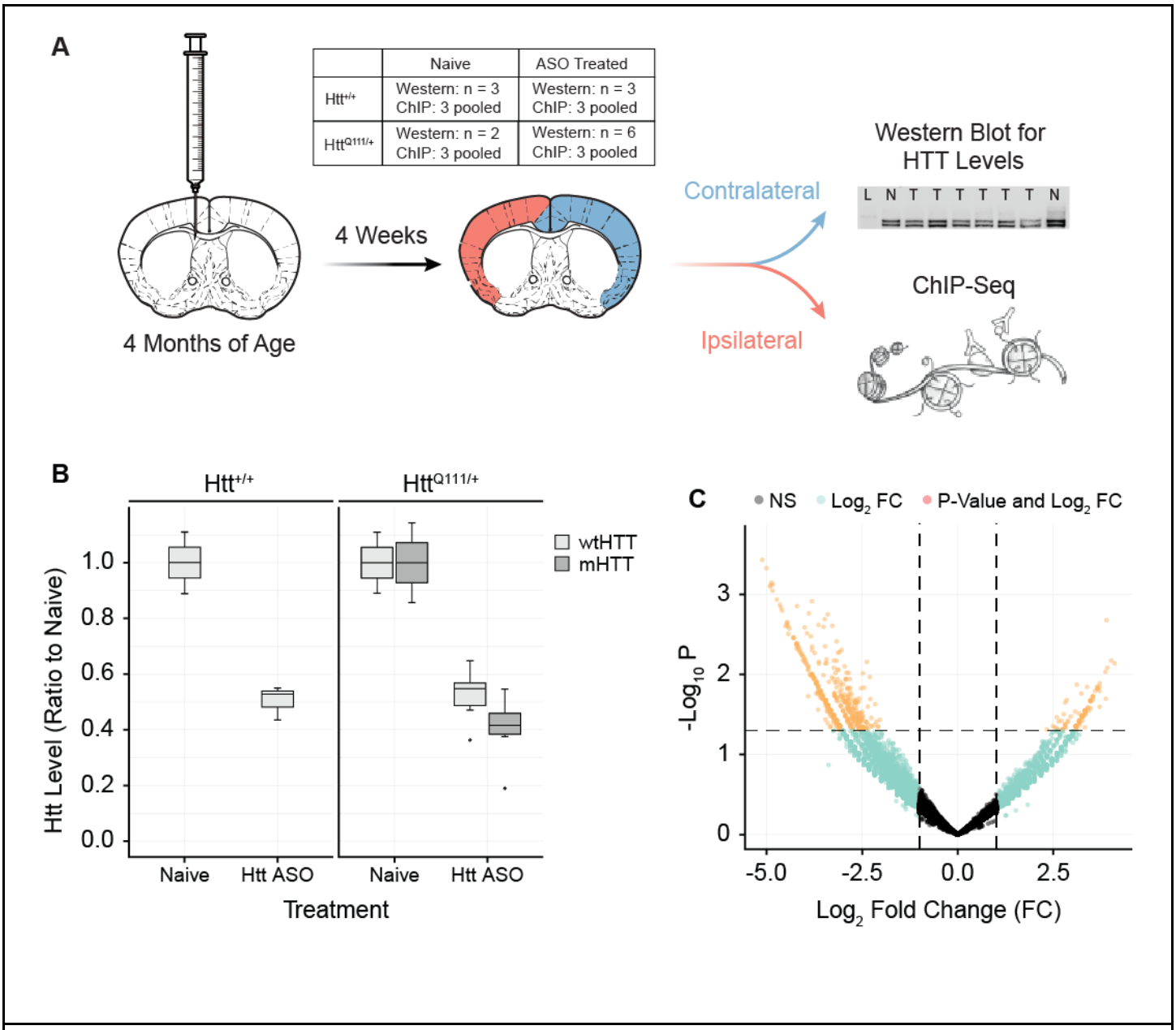

Supplementary Figure 1: Treatment with a HTT-lowering ASO reduces HTT ChIP-seq peaks. A) Mice underwent unilateral intracerebroventricular injection with HTT-targeted ASO. Cortex ipsi- and contralateral to the injection were collected at four weeks post-injection. HTT lowering was assessed in the contralateral cortex, while ChIP was performed on the ipsilateral cortex. B) Quantification of western blots probed with anti-HTT EPR5526 show HTT lowering of 53% in the contralateral cortex at four weeks post-ASO injection (ANOVA, Treatment effect p = 4.11e09). C) Volcano plot demonstrating 13,820 reproducible HTT-associated

peaks in the cortex, 8,308 (60%) showing Log_2(fold change) < 0 with ASO treatment. Likelihood that more than 50% had negative fold changes, p = 4.2e126 (binomial test). Of differentially occupied peaks (p < 0.05): 502 out of 622 had negative fold changes (80%) with ASO treatment. Despite the small sample size and partial HTT knockdown, we detected a global depletion of HTT occupancy in the cortex of mice treated with HTT-lowering ASOs.

Supplementary Table 1 – Significant HTT peak calling results, including proximal gene names, including genotype category labels. The "MACS Significant HTT Peaks" tab includes the MACS peak calling results - annotated with the most proximal gene and the distance to it. The "Peak.Label" column indicates whether each peak is in the category of "mHTT-specific", "WT-specific", or "WT-mHTT-shared" – see text for details on these categories.

Supplementary Table 2 – HTT Peaks Per Gene. A per-gene summary of HTT peaks across the categories of "mHTT-specific", "WT-specific", or "WT-mHTT-shared."

Supplementary Table 3 – HTT DiffBind. Differential HTT occupancy in *Htt*$^{Q111/Q111}$ *vs. Htt*$^{+/+}$. Used to generate volcano plot Fig. 2A.

Supplementary Table 4 – HTT DiffBind Enrichr Results. Geneset enrichment results for differential HTT peak occupancy in Figs. 2B, 2C.

Supplementary Table 5 – DiffBind Summary ActiveMotif. Differential occupancy of EZH2, H3K27ac, H3K27me3, H3K4me3, and H3K9me3, peak regions. These results were used to generate Fig. 3A.

Supplementary Table 6 – H3K27me3 Enrichment. Enrichment of H3K27me3 peaks with lower occupancy in *Htt*$^{Q111/+}$ *vs. Htt*$^{+/+}$striatum (p < 0.005) assessed for enrichment using `Enrichr`. Tabs correspond to terms for

503 Gene Ontology Biological Process (GOBP), Gene Ontology Molecular Function (GOMF), and ENCODE and
504 ChEA Consensus Transcription Factors (ENCODE-CHEA_tfs). Used to generate Figs. 3B-D.
505
506 **Supplementary Table 7 – HTT Enrichment ActiveMotif Peaks.** Summary of `GAT` results testing the
507 enrichment of HTT ChIP-seq peaksets amongst EZH2, H3K27ac, H3K27me3, H3K4me3, and H3K9me3, peak
508 regions. These results were used to generate Fig. 3E.
509
510 **Supplementary Table 8 - HTT Peaks, ActiveMotif and RNASeq Integration.** Includes integrated ChIP-seq
511 and RNA-seq data for all intervals containing robust HTT peaks. For each HTT peak ("PeakRegion.ID"),
512 available changes in RNA expression of included genes ("Langfelder et. al. RNA-Seq") and our other ChIP-seq
513 data ("Re-analysis of ActiveMotif ChIP-Seq") are shown. These results were used to generate Fig. 5A-B and
514 6A-C.
515 **Supplementary Table 9 - HTT HDSigDB Overlap.** Includes enrichments for HTT Peak sets and the genes
516 included in each HDSigDB gene set. HDSigDB gene set meta information is included on the tab
517 "HDSigDB.Genesets". These results were used to generate Fig. 5C.
518

519 References

520 1. A novel gene containing a trinucleotide repeat that is expanded and unstable on Huntington's disease
521 chromosomes. The Huntington's Disease Collaborative Research Group. Cell. 1993;72: 971–983.

522 2. Bates GP, Dorsey R, Gusella JF, Hayden MR, Kay C, Leavitt BR, et al. Huntington disease. Nat Rev Dis
523 Primers. 2015;1: 15005.

524 3. Cha J-HJ. Transcriptional signatures in Huntington's disease. Prog Neurobiol. 2007;83: 228–248.

525 4. Achour M, Le Gras S, Keime C, Parmentier F, Lejeune F-X, Boutillier A-L, et al. Neuronal identity genes
526 regulated by super-enhancers are preferentially down-regulated in the striatum of Huntington's disease

527 mice. Hum Mol Genet. 2015;24: 3481–3496.

528 5. Bassi S, Tripathi T, Monziani A, Di Leva F, Biagioli M. Epigenetics of Huntington's Disease. Adv Exp Med
529 Biol. 2017;978: 277–299.

530 6. Le Gras S, Keime C, Anthony A, Lotz C, De Longprez L, Brouillet E, et al. Altered enhancer transcription
531 underlies Huntington's disease striatal transcriptional signature. Sci Rep. 2017;7: 42875.

532 7. Alcalá-Vida R, Seguin J, Lotz C, Molitor AM, Irastorza-Azcarate I, Awada A, et al. Age-related and disease
533 locus-specific mechanisms contribute to early remodelling of chromatin structure in Huntington's disease
534 mice. Nat Commun. 2021;12: 1–16.

535 8. Ament SA, Pearl JR, Grindeland A, St Claire J, Earls JC, Kovalenko M, et al. High resolution time-course
536 mapping of early transcriptomic, molecular and cellular phenotypes in Huntington's disease CAG knock-in
537 mice across multiple genetic backgrounds. Hum Mol Genet. 2017;26: 913–922.

538 9. Hodges A, Strand AD, Aragaki AK, Kuhn A, Sengstag T, Hughes G, et al. Regional and cellular gene
539 expression changes in human Huntington's disease brain. Hum Mol Genet. 2006;15: 965–977.

540 10. Langfelder P, Cantle JP, Chatzopoulou D, Wang N, Gao F, Al-Ramahi I, et al. Integrated genomics and
541 proteomics define huntingtin CAG length-dependent networks in mice. Nat Neurosci. 2016;19: 623–633.

542 11. Xia J, Lee DH, Taylor J, Vandelft M, Truant R. Huntingtin contains a highly conserved nuclear export
543 signal. Hum Mol Genet. 2003;12: 1393–1403.

544 12. Gu X, Cantle JP, Greiner ER, Lee CYD, Barth AM, Gao F, et al. N17 Modifies mutant Huntingtin nuclear
545 pathogenesis and severity of disease in HD BAC transgenic mice. Neuron. 2015;85: 726–741.

546 13. Saudou F, Finkbeiner S, Devys D, Greenberg ME. Huntingtin acts in the nucleus to induce apoptosis but
547 death does not correlate with the formation of intranuclear inclusions. Cell. 1998;95: 55–66.

548 14. Benn CL, Sun T, Sadri-Vakili G, McFarland KN, DiRocco DP, Yohrling GJ, et al. Huntingtin modulates
549 transcription, occupies gene promoters in vivo, and binds directly to DNA in a polyglutamine-dependent
550 manner. J Neurosci. 2008;28: 10720–10733.

551 15. Neuwald AF, Hirano T. HEAT repeats associated with condensins, cohesins, and other complexes
552 involved in chromosome-related functions. Genome Res. 2000;10: 1445–1452.

553 16. Saudou F, Humbert S. The Biology of Huntingtin. Neuron. 2016;89: 910–926.

554 17. Seong IS, Woda JM, Song J-J, Lloret A, Abeyrathne PD, Woo CJ, et al. Huntingtin facilitates polycomb
555 repressive complex 2. Hum Mol Genet. 2010;19: 573–583.

556 18. von Schimmelmann M, Feinberg PA, Sullivan JM, Ku SM, Badimon A, Duff MK, et al. Polycomb
557 repressive complex 2 (PRC2) silences genes responsible for neurodegeneration. Nat Neurosci. 2016;19:
558 1321–1330.

559 19. Malaiya S, Cortes-Gutierrez M, Herb BR, Coffey SR, Legg SRW, Cantle JP, et al. Single-Nucleus RNA-
560 Seq Reveals Dysregulation of Striatal Cell Identity Due to Huntington's Disease Mutations. J Neurosci.
561 2021;41: 5534–5552.

562 20. Margueron R, Reinberg D. The Polycomb complex PRC2 and its mark in life. Nature. 2011;469: 343–349.

563 21. Bragg RM, Coffey SR, Weston RM, Ament SA, Cantle JP, Minnig S, et al. Motivational, proteostatic and
564 transcriptional deficits precede synapse loss, gliosis and neurodegeneration in the B6.Htt model of
565 Huntington's disease. Sci Rep. 2017;7: 41570.

566 22. Schut MH, Pepers BA, Klooster R, van der Maarel SM, El Khatabi M, Verrips T, et al. Selection and
567 characterization of llama single domain antibodies against N-terminal huntingtin. Neurol Sci. 2015;36:
568 429–434.

569 23. Zhang Y, Liu T, Meyer CA, Eeckhoute J, Johnson DS, Bernstein BE, et al. Model-based analysis of ChIP-
570 Seq (MACS). Genome Biol. 2008;9: R137.

571 24. Yu G, Wang L-G, He Q-Y. ChIPseeker: an R/Bioconductor package for ChIP peak annotation, comparison
572 and visualization. Bioinformatics. 2015;31: 2382–2383.

573 25. Ross-Innes CS, Stark R, Teschendorff AE, Holmes KA, Ali HR, Dunning MJ, et al. Differential oestrogen
574 receptor binding is associated with clinical outcome in breast cancer. Nature. 2012;481: 389–393.

575 26. Xie Z, Bailey A, Kuleshov MV, Clarke DJB, Evangelista JE, Jenkins SL, et al. Gene Set Knowledge
576 Discovery with Enrichr. Curr Protoc. 2021;1: e90.

577 27. Wu C, Jin X, Tsueng G, Afrasiabi C, Su AI. BioGPS: building your own mash-up of gene annotations and
578 expression profiles. Nucleic Acids Res. 2016;44: D313–6.

579 28. McLean CY, Bristor D, Hiller M, Clarke SL, Schaar BT, Lowe CB, et al. GREAT improves functional
580 interpretation of cis-regulatory regions. Nat Biotechnol. 2010;28: 495–501.

581 29. Liu Y, Li G. Empowering biologists to decode omics data: the Genekitr R package and web server. BMC
582 Bioinformatics. 2023;24: 214.

583 30. Pereira JD, Sansom SN, Smith J, Dobenecker M-W, Tarakhovsky A, Livesey FJ. Ezh2, the histone
584 methyltransferase of PRC2, regulates the balance between self-renewal and differentiation in the cerebral
585 cortex. Proc Natl Acad Sci U S A. 2010;107: 15957–15962.

586 31. Plaisier CL, O'Brien S, Bernard B, Reynolds S, Simon Z, Toledo CM, et al. Causal Mechanistic Regulatory
587 Network for Glioblastoma Deciphered Using Systems Genetics Network Analysis. Cell Syst. 2016;3: 172–
588 186.

589 32. Ament SA, Pearl JR, Cantle JP, Bragg RM, Skene PJ, Coffey SR, et al. Transcriptional regulatory
590 networks underlying gene expression changes in Huntington's disease. Mol Syst Biol. 2018;14: e7435.

591 33. Steffan JS, Kazantsev A, Spasic-Boskovic O, Greenwald M, Zhu YZ, Gohler H, et al. The Huntington's
592 disease protein interacts with p53 and CREB-binding protein and represses transcription. Proc Natl Acad
593 Sci U S A. 2000;97: 6763–6768.

594 34. Bannister AJ, Schneider R, Myers FA, Thorne AW, Crane-Robinson C, Kouzarides T. Spatial distribution
595 of di- and tri-methyl lysine 36 of histone H3 at active genes. J Biol Chem. 2005;280: 17732–17736.

596 35. Vakoc CR, Sachdeva MM, Wang H, Blobel GA. Profile of histone lysine methylation across transcribed
597 mammalian chromatin. Mol Cell Biol. 2006;26: 9185–9195.

598 36. Xiao T, Shibata Y, Rao B, Laribee RN, O'Rourke R, Buck MJ, et al. The RNA polymerase II kinase Ctk1

599 regulates positioning of a 5' histone methylation boundary along genes. Mol Cell Biol. 2007;27: 721–731.

600 37. Barrera LO, Li Z, Smith AD, Arden KC, Cavenee WK, Zhang MQ, et al. Genome-wide mapping and
601 analysis of active promoters in mouse embryonic stem cells and adult organs. Genome Res. 2008;18: 46–
602 59.

603 38. ENCODE Project Consortium. An integrated encyclopedia of DNA elements in the human genome.
604 Nature. 2012;489: 57–74.

605 39. Luo Y, Hitz BC, Gabdank I, Hilton JA, Kagda MS, Lam B, et al. New developments on the Encyclopedia of
606 DNA Elements (ENCODE) data portal. Nucleic Acids Res. 2020;48: D882–D889.

607 40. Zala D, Hinckelmann M-V, Yu H, Lyra da Cunha MM, Liot G, Cordelières FP, et al. Vesicular glycolysis
608 provides on-board energy for fast axonal transport. Cell. 2013;152: 479–491.

609 41. Truant R, Atwal RS, Burtnik A. Nucleocytoplasmic trafficking and transcription effects of huntingtin in
610 Huntington's disease. Prog Neurobiol. 2007;83: 211–227.

611 42. Zuccato C, Tartari M, Crotti A, Goffredo D, Valenza M, Conti L, et al. Huntingtin interacts with REST/NRSF
612 to modulate the transcription of NRSE-controlled neuronal genes. Nat Genet. 2003;35: 76–83.

613 43. Dietrich N, Lerdrup M, Landt E, Agrawal-Singh S, Bak M, Tommerup N, et al. REST-mediated recruitment
614 of polycomb repressor complexes in mammalian cells. PLoS Genet. 2012;8: e1002494.

615 44. Bodega B, Marasca F, Ranzani V, Cherubini A, Della Valle F, Neguembor MV, et al. A cytosolic Ezh1
616 isoform modulates a PRC2-Ezh1 epigenetic adaptive response in postmitotic cells. Nat Struct Mol Biol.
617 2017;24: 444–452.

618 45. Song W, Zsindely N, Faragó A, Marsh JL, Bodai L. Systematic genetic interaction studies identify histone
619 demethylase Utx as potential target for ameliorating Huntington's disease. Hum Mol Genet. 2018;27: 649–
620 666.

621 46. Rotem A, Ram O, Shoresh N, Sperling RA, Goren A, Weitz DA, et al. Single-cell ChIP-seq reveals cell
622 subpopulations defined by chromatin state. Nature Biotechnology. 2015. pp. 1165–1172.

623 doi:10.1038/nbt.3383

624 47. Kordasiewicz HB, Stanek LM, Wancewicz EV, Mazur C, McAlonis MM, Pytel KA, et al. Sustained
625 therapeutic reversal of Huntington's disease by transient repression of huntingtin synthesis. Neuron.
626 2012;74: 1031–1044.

627 48. Coffey SR, Bragg RM, Minnig S, Ament SA, Cantle JP, Glickenhaus A, et al. Peripheral huntingtin
628 silencing does not ameliorate central signs of disease in the B6.HttQ111/+ mouse model of Huntington's
629 disease. PLoS One. 2017;12: e0175968.

630 49. Skene PJ, Henikoff S. A simple method for generating high-resolution maps of genome-wide protein
631 binding. Elife. 2015;4: e09225.

632 50. Langmead B, Salzberg SL. Fast gapped-read alignment with Bowtie 2. Nat Methods. 2012;9: 357–359.

633 51. Amemiya HM, Kundaje A, Boyle AP. The ENCODE Blacklist: Identification of Problematic Regions of the
634 Genome. Sci Rep. 2019;9: 9354.

635 52. Li H, Handsaker B, Wysoker A, Fennell T, Ruan J, Homer N, et al. The Sequence Alignment/Map format
636 and SAMtools. Bioinformatics. 2009;25: 2078–2079.

637 53. Egan B, Yuan C-C, Craske ML, Labhart P, Guler GD, Arnott D, et al. An Alternative Approach to ChIP-Seq
638 Normalization Enables Detection of Genome-Wide Changes in Histone H3 Lysine 27 Trimethylation upon
639 EZH2 Inhibition. PLOS ONE. 2016. p. e0166438. doi:10.1371/journal.pone.0166438

640 54. Robinson MD, McCarthy DJ, Smyth GK. edgeR: a Bioconductor package for differential expression
641 analysis of digital gene expression data. Bioinformatics. 2010;26: 139–140.

642 55. Heger A, Webber C, Goodson M, Ponting CP, Lunter G. GAT: a simulation framework for testing the
643 association of genomic intervals. Bioinformatics. 2013. pp. 2046–2048. doi:10.1093/bioinformatics/btt343

644